An MRI-Compatible Robotic System with Hybrid Tracking for MRI-Guided Prostate Intervention

Axel Krieger, *Member, IEEE*, Iulian I. Iordachita, *Member, IEEE*, Peter Guion, *Member, IEEE*, Anurag K. Singh M.D., Aradhana Kaushal M.D., Cynthia Ménard M.D., Peter A. Pinto M.D., Kevin Camphausen M.D., Gabor Fichtinger, *Member, IEEE*, Louis L. Whitcomb, *Fellow, IEEE*

***Abstract*—This paper reports the development, evaluation, and first clinical trials of the APT II system — a scanner independent system for magnetic resonance image (MRI) guided transrectal prostate interventions. The system utilizes novel manipulator mechanics employing a steerable needle channel and a novel six degree of freedom hybrid tracking method, comprised of passive fiducial tracking for initial registration and subsequent incremental motion measurements. Targeting accuracy of the system in prostate phantom experiments and two clinical human-subject procedures is shown to compare favorably with existing systems using passive and active tracking methods. The portable design of the APT II system, using only standard MRI image sequences and minimal custom scanner interfacing, allows the system to be easily used on different MRI scanners.**

***Index Terms*—Magnetic resonance imaging, robot manipulators, image-guided intervention, prostate cancer.**

I. Introduction

We report the development and preliminary clinical evaluation of a scanner independent robotic system, called the APT II System, for magnetic resonance image (MRI) guided transrectal prostate interventions such as needle biopsy, fiducial marker placement, and therapy delivery. The system utilizes a novel manipulator, Figure 1, employing a steerable needle channel and a novel six degree of freedom (6-DOF) hybrid tracking method comprised of passive fiducial tracking for initial registration and subsequent incremental motion measurement along the degrees of freedom using fiber optical encoders and mechanical scales. Phantom and clinical targeting accuracy and procedure times are shown to compare favorably with existing systems using passive tracking (in which pose of the device is determined through passive imaging of embedded fiducials) and active tracking methods (in which pose of the device is measured through an active sensor e.g. magnetic resonance (MR) tracking coil).

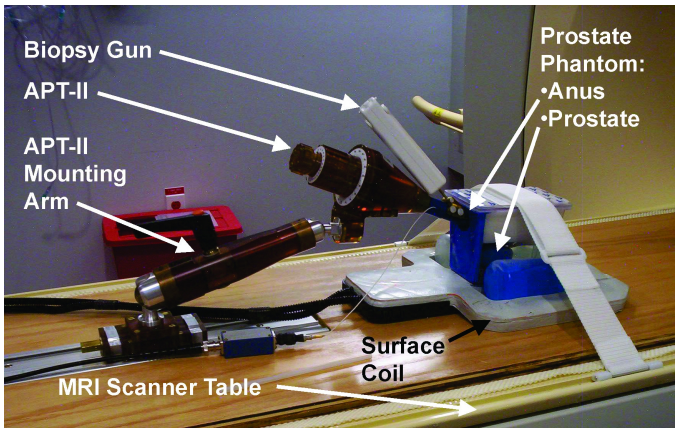

Fig. 1. Photograph of the MRI-guided transrectal manipulator of the The APT II system for MRI-guided transrectal needle access to the prostate showing the device's endorectal probe inserted in a prostate phantom.

The APT II hybrid tracking method solves a significant practical problem with the APT I system, [1], namely the APT I's need for custom active tracking MR scanner sequences. Moreover, this hybrid tracking method is applicable to other image-guided interventions. There is a strong present need for an MRI-guided prostate intervention system as a research validation tool. In particular, MR spectroscopy (MRS), dynamic contrast enhancement (DCE-MRI), and diffusion weighted imaging (DWI) are rapidly developing MRI modalities whose capabilities in finding cancerous lesions in the prostate can be tested using this intervention system.

Reported herein are the results of the first two clinical procedures with human subjects performed with the APT II system at the National Institutes of Health (NIH) Radiation Oncology Branch (ROB) in Bethesda, Maryland. APT II systems have been deployed at the following three clinical sites: (i) the NIH ROB, (ii) the Radiation Oncology Department at Princess Margaret Hospital (PMH) in Toronto, and (iii) the Johns Hopkins University (JHU) Department of Radiology. Each clinical site uses a different MRI scanner and employs a different clinical protocol. The APT II system received

Manuscript received September 19, 2010; Revised November 11, 2010 and January 31, 2011; Accepted February 2, 2011.

A. Krieger was with the Department of Mechanical Engineering (ME) and Laboratory for Computational Sensing and Robotics (LCSR), Johns Hopkins University (JHU), Baltimore, Maryland, USA and is presently with Sentinelle Medical Inc., Toronto, Canada. I. Iordachita and L. L. Whitcomb are with the JHU LCSR and JHU ME. P. Guion, A. Singh, K. Camphausen, and A. Kaushal are with the Radiation Oncology Branch (ROB), National Cancer Institute (NCI), National Institutes of Health (NIH), Bethesda, Maryland, USA. A. K. Singh was with the ROB NCI NIH, Bethesda, Maryland, USA and is presently with the Roswell Park Cancer Institute, Buffalo, NY, USA. P. A. Pinto is with the Urologic Oncology Branch, NCI NIH, Bethesda, Maryland, USA. C. Ménard is with the Radiation Oncology Department at Princess Margaret Hospital, Toronto, Canada. G. Fichtinger is with the School of Computing, Queen's University, Kingston, Ontario, Canada. The Johns Hopkins University has licensed intellectual property for the device and system described herein to Sentinelle Medical Inc., Toronto, Canada.

This research was supported by the National Institutes of Health under Grant RO1-EB02963 to the Johns Hopkins University. Gabor Fichtinger was funded as Cancer Care Ontario Research Chair.

non-significant risk determination from the Food and Drug Administration (FDA) in conjunction with clinical protocols at the NIH. The system received Internal Review Board (IRB) approvals at NIH, PMH, and JHU with their respective clinical protocols. The protocol for PMH was also approved by Health Canada. To date, the APT II system has been employed in 15 patient cases at NIH, PMH, and JHU. Our previous-generation APT I system was employed in 37 clinical human-subject trials at NIH [1]–[4]. We have employed the APT II on different 1.5T and 3.0T closed-bore MRI scanners manufactured by Siemens, General Electric, and Phillips. Clinical studies using the APT II are ongoing at NIH, PMH, and JHU.

II. Prostate Cancer Diagnosis and Therapy

Prostate cancer is the most common cancer in men in the United States. In the United States in 2010, an estimated 217,730 men will be diagnosed with prostate cancer and 32,050 will die of this disease [5]. 1 in 6 U.S. men contract prostate cancer during their lifetime, and 1 in 36 U.S. men die of this disease. Approximately 1.2 million prostate biopsy procedures are performed annually in the U.S. [6], [7].

A. Ultrasound-Guided Prostate Intervention

The present-day definitive diagnosis for prostate cancer is core needle biopsy, pursuant to either an elevated prostate-specific antigen (PSA) blood level or a positive rectal exam (DRE). The "Gold Standard" of guiding biopsy, as well as of most local therapies, is transrectal ultrasound (TRUS) image guidance [8]. The physician manually places a TRUS probe in the rectum and, under ultrasound guidance, inserts a biopsy needle through the wall of the rectum into the prostate gland. The needle removes a half-cylinder of tissue, which is examined pathologically to determine if cancer is present. Several biopsy samples are taken from different areas of the prostate. Usually six (hence "sextant biopsy") to eighteen cores are removed from upper, mid, and lower areas of the left and right sides to obtain a representative sampling of the gland and determine the degree and extent of cancer.

TRUS-guided prostate biopsy is widely employed due to its real-time nature, relatively low cost, and ease of use. Its limitations, however, are substantial. Although shortcomings have been known over a decade and often reconfirmed, there are no major improvements in sight. Using standard techniques, biopsy of men with PSA blood test values in the range of 4-10 ng/ml generally result in a cancer detection rate of 20%-30% [9], [10]. Numerous studies have shown that TRUS-guided prostate biopsy fails to detect cancer in at least 20% of patients with cancer [11]–[14]. Studies report that TRUS-guided biopsies are limited by low sensitivity of 60% with only 25% positive predictive value, in which no significant change has been seen, for example, by Terris et al. in the past 15 years [15]. Such observations have been corroborated by many, including [7], [16]–[19]. For example Gann et. al. report "Seventy to 80% of the approximately 1.2 million patients who undergo prostate biopsy each year in the United States receive negative results (i.e., no cancer) but cannot be completely reassured because a cancer may have been missed by [TRUS-guided biopsy] sampling error" [7]. Studies have shown that more than one-third of men whose first biopsies were negative were re-biopsied within the next 5 years, resulting in a large number of repeat biopsy cases [19]. Despite advances in ultrasound imaging methods, TRUS imaging is generally unable to differentiate between healthy tissue and cancerous lesions in the prostate. In consequence, contemporary TRUS-guided biopsy cannot identify or target lesions, and cancerous nodes of clinically significant size are routinely missed. Clearly, significantly improved alternatives to TRUS image guidance are needed.

B. The Case for MRI-Guided Prostate Intervention

MRI possesses many of the capabilities that TRUS is lacking. MRI is an attractive choice for image-guidance, primarily due to its high sensitivity for detecting prostate tumors [13], [20]–[23], high spatial resolution, excellent soft tissue contrast, and volumetric imaging capabilities.

Advances in pelvic and endorectal coils have dramatically enhanced the ability of MRI to visualize prostate tissues [24], [25]. MRI can clearly visualize the prostate and its substructure including the peripheral zone (PZ). As the PZ is the most common site of origin of prostate cancer, localizing and targeting suspicious PZ lesions during prostate biopsy is expected to increase cancer detection rate. T2 weighted images can identify suspicious nodules in the prostate, allowing targeted biopsy and subsequent local therapy.

Several novel MRI methods are currently being developed in an effort to improve the specificity of prostate cancer detection and characterization, including MR spectroscopy [13], [26], dynamic contrast enhancement, T2 maps, and diffusion imaging [27], [28]. MRI can visualize the distribution and buildup of injected liquid agents in the prostate [29], [30], and solid capsules [29], [31]. MRI can also monitor the progress of thermal therapies in real-time [32], [33].

C. Previously Reported MRI-Compatible Prostate Intervention Systems

This section reviews previously reported MRI-compatible systems for prostate intervention.

1) Transrectal Approach: In [1], [3], [4], [29], [30], [34], [35] the authors reported the development and clinical evaluation of a MRI-guided system for transrectal prostate biopsies, therapy injection, and marker placements. The system, called the APT I, contains a single-loop MRI endorectal imaging coil and employs active tracking for device localization. In vivo and in vitro accuracy results were reported. This APT-I clinical system has been successfully used in 37 patient procedures to date. To the best of our knowledge, the APT-I system is the only clinically utilized systems for transrectal MRI-guided access to the prostate employing active tracking.

In [36] Beyersdorff and in [37] Engelhard report MRI-guided transrectal needle biopsies in clinical studies with a system (InVivo Germany GmbH, Schwerin, Germany) employing manual alignment and passive tracking of a needle sleeve. In [38] Barentsz reports phantom studies with a MRI-compatible pneumatically actuated transrectal robot. Elhawary reported

phantom experiments with a prototype robotic system using piezo-ceramic motors for transrectal prostate biopsy [39].

2) Transperineal Approach: MRI-guided transperineal prostate intervention has been demonstrated in clinical studies inside an open MRI scanner [31] and conventional closed MRI scanner with the use of static needle-guiding templates [40]. A surgical assistant robot reported by Chinzei [41] was adapted to assist transperineal intra-prostatic needle placement [42]. Tadakuma reported the use of dielectric elastomer actuators in a pre-clinical prototype MRI-compatible robot for transperineal needle placement in the prostate [43], [44]. Stoianovici reported phantom experiments with a pneumatically actuated device for transperineal brachytherapy seed placement [45]. In [46] and [47] we reported the development of a device with a pneumatically actuated needle guide and manual needle insertion for transperineal needle placement in the prostate, and reported phantom experiments. Goldenberg reported phantom studies with a robotic system employing ultrasonic actuators in closed MRI scanners [48]. In [49] van den Bosch reported a hydraulically and pneumatically actuated tapping robot.

3) Transgluteal Approach: Zangos reported preliminary clinical results with 25 patients using the transgluteal approach with an open configuration 0.2 T MRI scanner, with targeting based on T1 and T2 diagnostic images previously acquired with a 1.5 T scanner [50]. However, they did not detail the technique used for the fusion of high-field diagnostic and low-field intra-operative MRI sequences. Zangos and Vogl reported usage of the Innomotion pneumatic robot in a cadaver study at 1.5 T for transgluteal prostate needle placements [51], and transgluteal MRI-guided galvanotherapy [52].

D. Clinically Significant Prostate Cancer Tumor Size

Prostate cancer is a progressive disease. As tumor volume increases, so does malignant potential. McNeal *et al.* found that metastasis occurs only in prostate cancer tumors larger than 4 ml and with Gleason Grades[1] of 4 or 5 [54]. A 0.5 ml prostate cancer volume has been proposed as the limit of clinically significant prostate cancer foci volume [16], [55] Assuming spherical shaped tumors, a 0.5 ml tumor volume corresponds to a sphere with diameter 9.8 mm. We conclude that an MRI-guided biopsy system employing a targeting accuracy of about 5 mm or better could reliably access clinically significant prostate cancer foci.

III. Novel 6-DOF Hybrid Tracking Method

The development of MRI-guided robotic intervention instruments is complicated by the need to track in real-time the pose (i.e. position and orientation) of these instruments within the MRI scanner. This section reviews previously reported tracking methods and reports the design and performance of the proposed hybrid tracking method.

A. Previously Reported Tracking Methods

Previously reported approaches for tracking of robotic and manual instruments within MRI scanners are as follows:

[1]The Gleason Grade is a widely used system for grading cell differentiation (cancer severity) in prostate cancer tissue samples. [53].

1) Joint Encoder Tracking: In this approach, the pose of the intervention device (e.g. needle or other surgical device) is determined by joint encoders at the device's articulated joints [41], [56], [57] This approach requires the addition of a custom rigid mechanical mounting system to the MRI scanner, and a precise pre-calibration of the device with respect to the scanner coordinate system.

2) Passive MRI Fiducial Feature Tracking: In this approach, the pose of the intervention device is is determined by localizing passive fiducial markers embedded within the device. Susil et al. developed a passive needle guiding template for transperineal MRI-guided prostate brachytherapy, where the template holes were filled with contrast material, pre-operatively localized in standard T1 or T2-weighted images, and registered to the coordinate frame of the MRI scanner [2], [40]. Beyersdorff et al. reported a MRI-guided transrectal needle biopsy system which employs a passive fiducial marker sleeve coaxial with the biopsy needle [36].

3) Optical Pose Tracking: In this approach, the pose of the intervention device is determined by an optical tracking system deployed and calibrated to the scanner coordinate system. This approach requires line-of-sight between the optical tracking cameras and the device, and requires passive optical targets or tethered light emitting diodes (LEDs) to be attached to the instrument. DiMaio et al. employed an optical tracker with an open MRI scanner to register the end-effector of an interventional robot to the MRI coordinate system [42].

4) Gradient Field Sensing: In this approach, the pose of the intervention device is determined by a tethered 3-axis magnetic sensor embedded within the device that senses the scanner gradient fields. Hushek et al. investigated an FDA-approved commercial tracking mechanism called EndoScout (Robin Medical Systems, Baltimore, MD) in an open MRI scanner [58]. In present implementations, the tracking sensors must be placed close to the MRI magnet's isocenter, and thus may occupy critical volume in the end-effector. This approach requires a precise one-time calibration procedure to be performed over the entire field of interest in each MRI system on which it is installed.

5) Micro Tracking Coils: In this approach, the pose of the intervention device is determined by three (or more) tethered micro-tracking coils that are embedded within the device to sense custom-programmed MRI pulse sequences. Micro-tracking coils, originally reported in [59], were employed on the APT I system [1], [29] to provide full 6-DOF tracking at 20 Hz. Its advantages are exceptionally fast and accurate (0.2 mm and 0.3°) 6-DOF instrument tracking. Its disadvantages are its lack of robustness due to the delicate micro-coils, the need for three (or more) dedicated scanner channels, and its need for custom-programmed tracking sequences that are not standard on commercial MRI scanners. The need for custom-programmed tracking sequences renders this approach impractical for widespread clinical deployment at present.

B. 6-DOF Hybrid Tracking of MRI-Compatible Instruments

This novel approach determines the pose of the intervention device by combining a one-time initial passive tracking

with MRI-compatible joint encoding to provide full 6-DOF instrument tracking throughout an MRI-guided interventional procedure. Our objective was to develop an alternative tracking methodology for the APT II system with the following performance goals: (i) measure 6-DOF pose with accuracy comparable to or surpassing previously reported approaches; (ii) employ only standard MRI pulse sequences; (iii) minimize embedded electronics; and (iv) MRI-compatibility with no imaging artifacts.

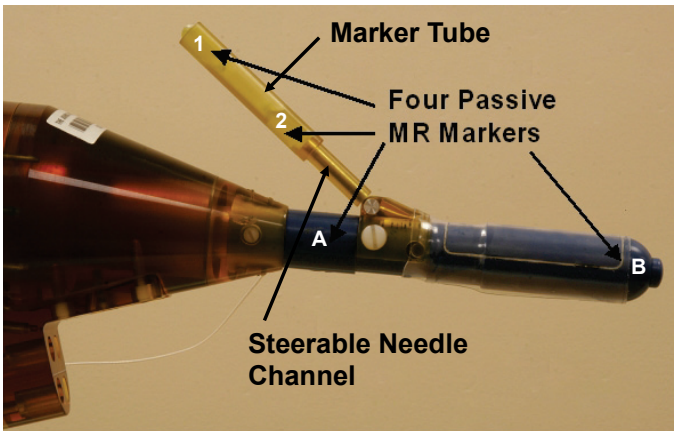

Fig. 2. Photograph of APT II system during initial registration. A marker tube is placed coaxially over the steerable needle channel. The tube contains two tubular markers, indicated as 1 and 2. Two additional markers, A and B, are placed into the main axis of the rectal sheath.

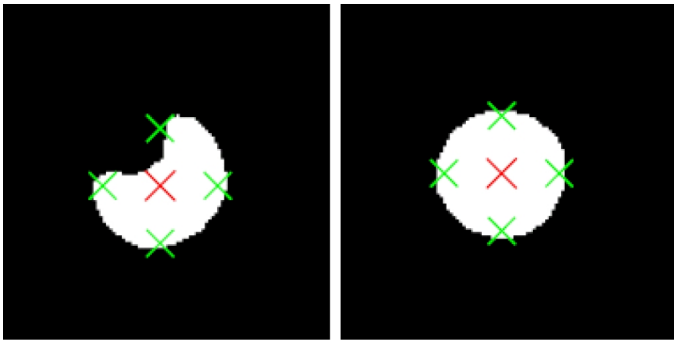

Fig. 3. Example of two binary reformatted PD weighted TSE images axial to a fiducial marker. The segmentation algorithm finds the best fitting circle center indicated by a big cross on both images. The algorithm is able to find the center, even when air bubbles in the marker on the left contaminate the image. Small crosses indicate the border of the marker.

The APT II hybrid tracking system, Figure 2, employs two gadolinium fiducial marker tubes incorporated into the main axis of the system and two marker tubes placed parallel to the needle channel. At the beginning of an interventional procedure, the initial pose of the APT II system in scanner coordinates is obtained by segmenting the four fiducial markers (Beekley Corp., Bristol, CT) placed on the APT II system in MRI images. From this initial pose, motion of the device along its axes is encoded with fiber-optical and manual encoders. A thin slab of 1 mm x 1 mm x 1 mm isotropic sagittal TSE proton density (PD) weighted images in the plane of the four markers is obtained with the scanner body coil. A robust

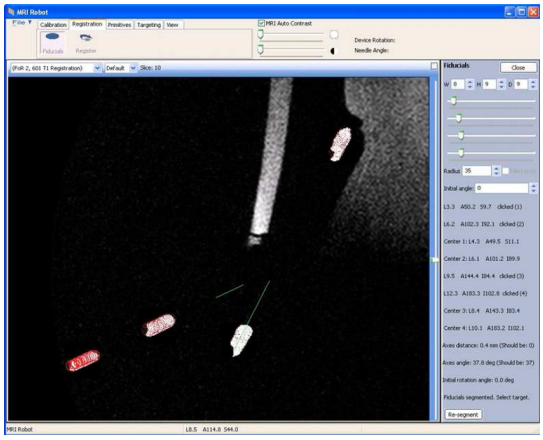

Fig. 4. Screen shot of the targeting program after a successful initial registration in a prostate phantom. The four segmented markers, indicated by red circles can be seen on the image, as well as the two green calculated lines, representing the endorectal probe axis and needle axis respectively.

segmentation algorithm based on the Hough transform, which finds on each binary reformatted image the best fitting center of a circle with known diameter, is employed to identify the centers of the four markers in multiple image slices normal to the marker axis (Figure 3). An algorithm was written based on the Hough transformation, which finds on each binary reformatted image the best fitting center of a circle with known diameter of the marker. This segmentation is very robust even on images containing air bubbles in the marker. The singular value decomposition (SVD), [60], is employed to compute the least-square best-fit lines, and to perform outlier rejection, for the needle channel axis and the endorectal probe axis (Figure 4). The two axes determine the 6-DOF pose of the manipulator in scanner coordinates.

As outlined in Section IV-B the three degrees of freedom to reach a target from this initial pose are rotation of the device, needle angle, and needle insertion. Rotation and needle angle change are redundantly encoded by MRI-compatible fiber-optic encoders and mechanical scales placed on the actuation knobs of the manipulator. The needle insertion depth is observed using the scale on the needle. This hybrid approach assumes that the APT-II device and the prostate remain motionless from the time of passive registration to the time of needle intervention. A confirmation scan can be taken immediately before to evaluate device and patient motion, and the device can be re-registered if significant motion is detected. The fiber optic joint encoders consist of photoelectric sensors (Banner Engineering Corp., Minneapolis, Minnesota) placed in a box in the control room, adjacent to the shielded MRI scanner room. A two-channel quadrature design with a third channel as index pulse is used for both encoders. Each sensor provides one channel, so six sensors are necessary to build the two encoders. Encoder resolution for rotation of the manipulator is 0.25°, and for needle angle less than 0.1° at all needle angles.

IV. APT II Robot Design

The APT II system, Figure 1, is a non-commercial research prototype consisting of the mechanical manipulator, a mount-

TABLE I
EXPERIMENTAL NEEDLE PLACEMENT ACCURACY TEST RESULTS
The left half of the table presents the results with all image slices for each marker used to calculate an axis. The right half contains accuracy entries where only one image slice per marker was used to calculate an axis.

Method of axes calculations	**All image slices for each marker**					**One image slice per marker**				
Markers used to define channel	"1, 2"	"1, 3"	"1, 4"	"3, 4"	"1,2,3,4"	"1, 2"	"1, 3"	"1, 4"	"3, 4"	"1,2,3,4"
Distance between markers (mm)	25	45	80	35	80	25	45	80	35	80
Mean angle α needle/device axis (°)	38.84°	38.74°	38.83°	38.94°	38.82°	38.62°	38.6°	38.73°	38.88°	38.74°
Std dev of angle α needle/device axis (°)	0.19°	0.14°	0.12°	0.18°	0.12°	0.23°	0.18°	0.15°	0.2°	0.14°
Max dev of angle α needle/device axis (°)	0.48°	0.33°	0.26°	0.37°	0.27°	0.46°	0.37°	0.29°	0.41°	0.3
Mean dist. d of intersection (mm)	51.77	51.59	51.75	51.68	51.71	51.51	51.48	51.68	51.63	51.63
Std dev of dist. d of intersection (mm)	0.19	0.2	0.17	0.16	0.16	0.3	0.2	0.2	0.2	0.19
Max dev of dist. d of intersection (mm)	0.52	0.41	0.26	0.29	0.26	0.66	0.38	0.37	0.35	0.32

ing arm, and a custom targeting software program.

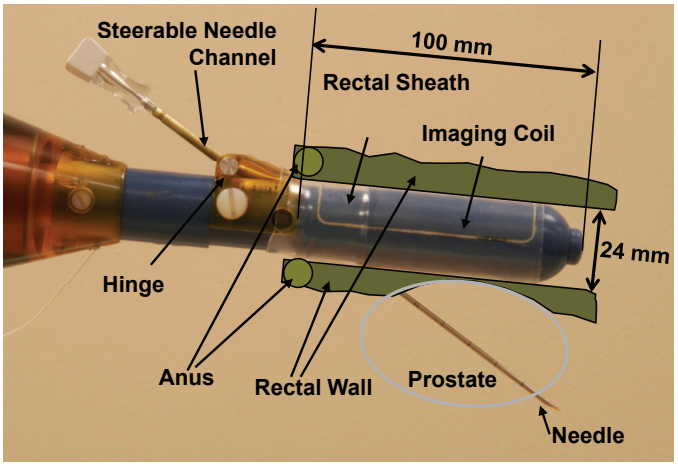

Fig. 5. Photograph of APT II steerable needle channel. The rectal sheath is inserted in the rectum, such that the hinge is placed close to the anus of the patient. The rectal sheath contains a single-loop imaging coil and a steerable needle channel.

A. Work flow

MRI-guided transrectal prostate biopsy procedures with the APT II are typically conducted as follows: (i) the patient is positioned and secured on the scanner table in a prone position (or supine position, depending on protocol), and the APT II probe is inserted into the patient's rectum; (ii) a thin sagittal volumetric MRI scan is taken to calibrate the APT II to the scanner coordinate system; (iii) optionally a volumetric MRI scan is taken to guide anesthetic injection; (iv) diagnostic MRI scans (e.g. T2, DCE, DWI, etc.) are taken, with which the clinician selects 4-12 biopsy target locations; (v) target locations are biopsied with the APT II; (vi) in some cases, fiducial markers are inserted at selected targets using the APT II. As with most MRI-guided interventions in closed MR scanners, the patient (still secured on the scanner table) is removed from the scanner bore for biopsy and marker insertion and, optionally, returned into the scanner bore for confirmation images of needle/marker placement; (vii) at the conclusion of the procedure, the APT II probe is removed from the patient's rectum and the patient is unsecured from the scanner table.

B. Steerable Needle Guide

Needle biopsy procedures with commercial biopsy needles, gold marker placements, and therapy delivery require a straight needle approach to the prostate. Figure 5 shows a photograph of the steerable needle guide of the APT II system. The rectal sheath is inserted in the rectum, such that the hinge is placed close to the exterior of the patient's anus. The rectal sheath contains a single-loop imaging coil, which is bonded into a machined groove on the sheath. The three DOF to reach a target inside the prostate are: rotation of rectal sheath, angulation change of the steerable needle guide, and insertion of the needle. A wide range of needle angles from 17.5° to 40° provides full prostate coverage for most patients.

C. Manipulator Design

A manually-actuated design for the manipulator was chosen over an automated design to minimize development time and regulatory approval time for clinical trials. Moreover, manual actuation for insertion of the needle is preferred by many physicians because it enables visual confirmation of the needle alignment before insertion and tactile feedback during the insertion of the needle.

Figure 1 shows the manipulator with its endorectal imaging coil placed in a prostate phantom (CIRS Inc, Norfolk, VA). The probe is positioned using an arm mounted on the scanner bed. The manipulator guides the needle tip of a standard automatic MRI-compatible biopsy gun (Invivo Germany GmbH, Schwerin, Germany) to a predetermined target in the prostate. A two-channel surface imaging coil is placed underneath the phantom to enhance the MRI signal, especially for the posterior part of the prostate.

Figure 6 shows a close up photograph of the manipulator. The sheath can be rotated 360°, thus allowing for a variety of patient positions including prone, supine, and decubitus.

Needle angle adjustment of the steerable needle channel is controlled by turning the smaller diameter knob on the manipulator. A narrow slot on the bottom of the endorectal sheath allows the needle to exit the sheath. Achievable needle angles (measured between manipulator axis and needle channel axis) range from 17.5° to 40°. The hinge is placed as close as possible to the anus of the patient, thus maximizing the needle angle for any given target in the prostate. A larger needle angle reduces the length the needle has to travel through the patient's tissue to reach the target. The endorectal sheath with the hinge

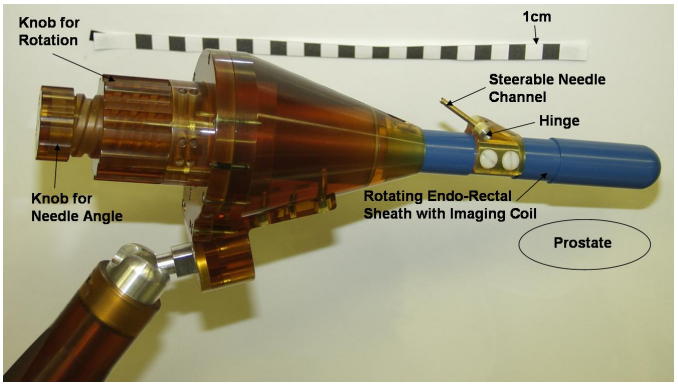

Fig. 6. Closeup photograph of the manipulator of the APT II system. Turning the knobs on the left rotates the endorectal sheath with the hinge and needle channel and changes the angle of the steerable needle channel, respectively. An endorectal, single-loop imaging coil is integrated into the sheath.

and needle channel are cleaned and sterilized before every procedure. The manipulator is constructed mostly of plastic materials, principally of Ultem (GE Plastics, Pittsfield, MA), selected for its structural stability, machinability and low cost.

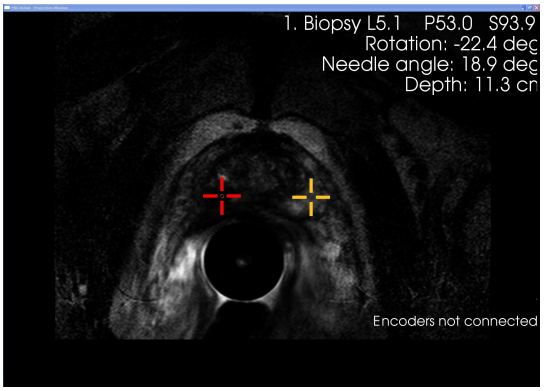

Fig. 7. Targeting Program: The red cross marks the currently selected target for needle placement in the prostate. Rotation, needle angle and insertion depth are displayed to reach the selected (red) target. The yellow mark is another target.

D. Targeting Program

A new custom-developed targeting program was written for the APT II system. The targeting software displays the acquired MRI images, provides the automatic segmentation for the initial registration of the manipulator, allows the physician to select targets for needle placements, provides targeting parameters for the placement of the needle, tracks rotation and needle angle change provided by the encoders, while the manipulator is moved on target, and logs data. Figure 7 shows a screen shot of a projection window provided by the targeting program. The red cross marks the desired target for needle placement in the prostate.

V. Experiments and Results

The APT II system for MRI-guided transrectal prostate interventions was tested in a phantom imaging test, phantom targeting experiments, and two human subject cases. Possible sources of image-guided needle targeting error include image resolution and pixel size, initial registration accuracy, patient motion, robot motion, encoding resolution, and tissue deformation [61], [62] All tests and procedures were performed on a 3.0T Philips Intera MRI scanner (Philips Medical Systems, Best, NL).

A. Experimental Evaluation of Hybrid Tracking Accuracy

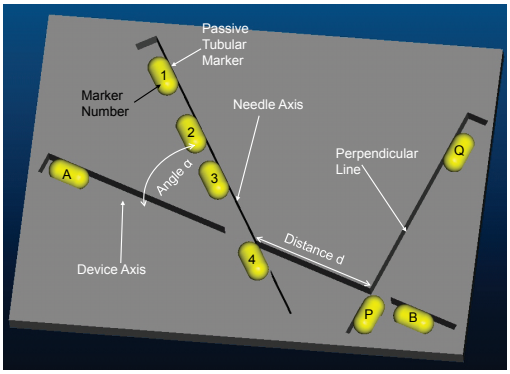

Fig. 8. CAD rendering of the test plate. The test plate contains machined grooves for the device axis, the needle axis, and a third perpendicular groove. Markers are placed in each channel. Markers 1,2, A, and B correspond to those employed in the APT II as indicated in Figure 2. The channels are machined with nominal angle $\alpha = 39°$ and distance d = 50 mm.

1) Experimental Setup: The accuracy of the passive tracking method for determining the initial device pose was tested in phantom experiments. A plate was built with three integrated channels (Figure 8): A channel representing the device axis, a channel for the needle axis at a 39° angle (angle α) to the device axis, and a channel perpendicular to the device axis placed 50 mm (distance d) away from the intersection point of the device and needle axis. Passive gadolinium marker tubes, (Beekley Corp., Bristol, CT), 8 mm in diameter and 15 mm long, were positioned along each axis.

The marker plate assembly was imaged in 16 different orientations with an isotropic 1 mm x 1 mm x 1 mm PD weighted TSE sagittal image sequence. The three line equations for the axes were calculated from the marker center locations, with a least squares fitting algorithm based on the singular value decomposition, and the distance d, angle α, and distance between axes (Figure 8) were computed.

2) Experimental Results: Table I shows the accuracy results for the 16 different orientations. On the left half of the table all recorded marker center locations were used to calculate each axis, on the right half of the table, only one center location for each marker was used. The standard and maximum deviation values in the right half of the table are only slightly higher than in the left half, indicating that only one location per marker yields satisfactory accuracy. Using all four markers to define the needle axis (in contrast to using markers 1 and 4 alone) only marginally improves accuracy.

3) Comparison of Micro-Coil and Passive Fiducial Tracking Accuracy: To compare the accuracy of the hybrid tracking method to the active tracking method, error histograms of 16

passive tracking orientations were obtained and compared to 36 active tracking orientations obtained for active tracking [1]. Since the hybrid tracking method is comprised of initial passive tracking and subsequent encoder tracking, an error model for the encoders was added to the passive tracking results. The optical encoders, which will be used for the tracking, have a resolution of $0.25°$. A random, zero mean error with uniform distribution and an amplitude of $0.25°$ was added to the passive tracking results to simulate the combined error of the hybrid tracking method. For the passive tracking error, the marker combination 1 and 3 with one circle per marker for segmentation was selected for comparison to the active tracking. Markers 1 and 3 are located at a distance of 45 mm from each other. Figure 9 shows histograms of angular errors for the active tracking (left) and the hybrid tracking (right). The accuracy results for the hybrid tracking method are satisfactory, considering that with a reasonable distance between markers of 45 mm, the maximum angular deviation lies at $0.6°$. This is below the $\pm$ 1° error for the active tracking.

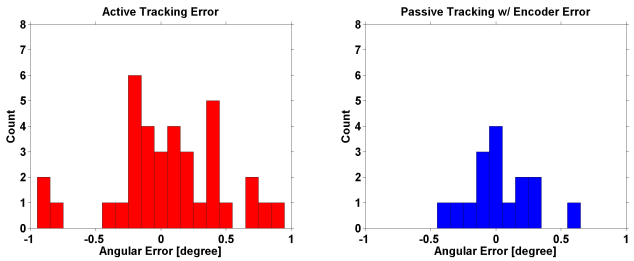

Fig. 9. Histograms for angular errors for 36 active tracking trials (left) and 16 hybrid tracking trials (right), comprised of passive and encoder tracking. Maximum and mean error are lower for the hybrid tracking method.

4) Experimental Evaluation of Hybrid Tracking Accuracy: The experimental results demonstrated that the hybrid tracking method can be used for accurate tracking of interventional robotic devices. Only one location per marker is enough to accurately compute an axis. Segmentation and consequent axis definition for initial pose tracking can be computed in a few seconds. Tracking errors compare favorably to active tracking, e.g. [1], [29], [59], but are more easily deployed since it utilizes only standard MRI pulse sequences.

B. Endorectal Coil Imaging Results

The APT II manipulator contains an endorectal imaging coil consisting of a single-turn coil integrated into the endorectal sheath. To assess the quality of the endorectal imaging coil, a signal to noise (SNR) comparison of the endorectal coil with a commercially available flexible endorectal coil (MedRad Inc., Indianola, PA) was performed. A 3.0 T Phillips Achieva scanner was used to obtain T2 weighted axial TSE MR volumetric sequences (TR of 9302 msec, TE of 180 msec, slice thickness of 3.5 mm, and Echo Train Length 21) of a 2.5 g/l saline phantom. The MR sequence was selected for SNR comparisons since the same sequence is used for selection of targets for biopsy procedures in the clinical protocol. The image slice with highest signal intensity in the acquired volume was used for SNR comparison. The noise value for the SNR was computed as the standard deviation of a rectangle uniform noise distribution in an area of the image containing only air above the phantom — the NEMA standard method [63]. Figure 10 shows SNR maps for both coils. Despite the smaller diameter of the APT endorectal coil, it yielded higher SNR than the MedRad flexible coil. The SNR comparison suggests that performing high-resolution diagnostic imaging of the prostate prior to an interventional procedure is possible with the proposed system.

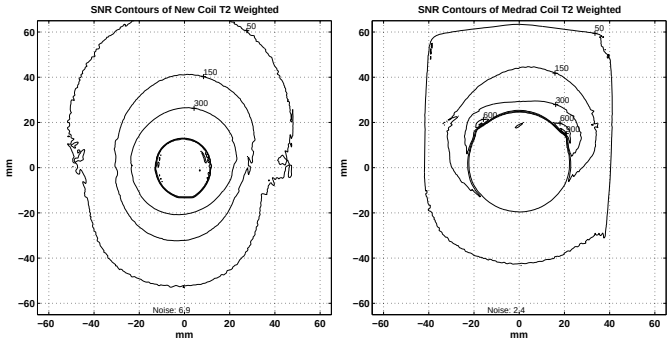

Fig. 10. T2 FSE SNR contours obtained with the APT II endorectal coil (left) and commercially available MedRad coil (right).

C. Phantom Needle Targeting Results

Phantom experiments were performed using standard MRI-compatible biopsy needles and artifact-free glass needles. The experimental setup is shown in Figure 1.

1) Biopsy Needle Placement Accuracy: The manipulator was placed in a prostate phantom and its initial pose was registered. Twelve targets were selected within all areas of the prostate, from base through mid gland to apex, on T2 weighted axial turbo spin echo (TSE) images (Figure 11, first and fourth row). All scans were axial with Anterior-Posterior frequency encoding and Left-Right phase encoding.

For each target, the targeting program calculated the necessary targeting parameters for the needle placement. The phantom was withdrawn from the MRI scanner on the scanner table, the operator rotated the manipulator, adjusted the needle angle, and inserted the biopsy needle according to the displayed parameters. The phantom was inserted into the scanner to confirm the location of the needle on axial TSE proton density images that show the MRI image void created by the biopsy needle tip close to the target point (Figure 11, second and fifth row). The in-plane error for each of the twelve biopsies, defined as the distance of the target to the biopsy needle axis was calculated to assess the accuracy of the system. The needle line was defined by finding the first and the last slice of the acquired confirmation volume, where the needle void is clearly visible. The center of the needle void on the first slice and the center of the void on the last slice define the needle line. The out-of-plane error is not critical in biopsy procedures, due to the length of the biopsy core, and was not calculated. The average in-plane error for the biopsy needles was 1.5 mm with a maximum error of 2.5 mm.

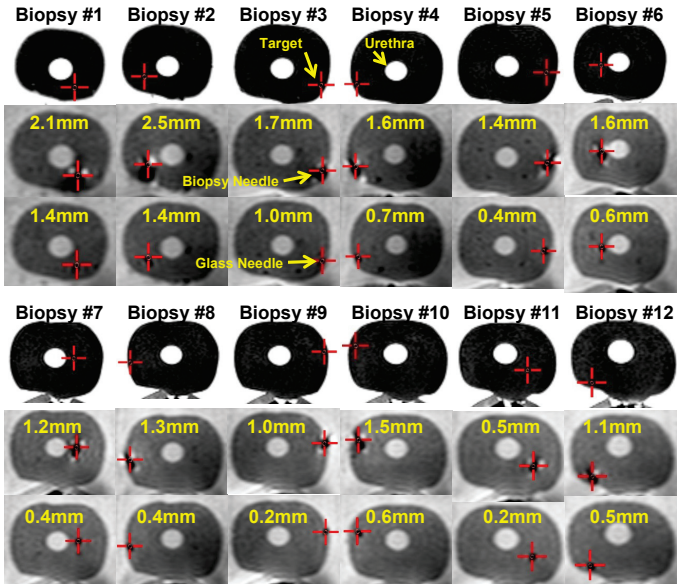

Fig. 11. Targeting images, biopsy needle confirmation images, glass needle confirmation images and in-plane errors for twelve biopsies of a prostate phantom using the APT II system. First and fourth row: A target (red cross-hair) is selected on axial TSE T2-weighted images. Second and fifth row: The biopsy needle tip void is visualized in an axial TSE proton density image. The desired target approximately matches the actual position of the needle. Third and last row: The glass needle tip void is visualized in an axial TSE proton density image. Numbers indicate the in-plane needle targeting error for the needle placement.

2) Glass Needle Accuracy: The MRI image void created by the biopsy needle is mostly due to susceptibility artifacts caused by the metallic needle. The void is not concentric around the biopsy needle and its location depends on the orientation of the needle to the direction of the main magnetic field in the scanner (B0), and the direction of the spatially encoding magnetic field gradients [42]. Consequently, centers of needle voids do not necessarily correspond to actual needle centers. And since the same imaging sequence and similar orientation of the needle is used for all targets in a procedure, a systematic shift between needle void and actual needle might occur, which introduces a bias in the accuracy calculations. To explore this issue, every biopsy needle placement in the prostate phantom was followed by a placement of a glass needle to the same depth. The MR image of the glass needle is artifact free and concentric to the needle, and does not exhibit the susceptibility artifacts observed with metallic needles. The location of the glass needle was confirmed by acquiring axial TSE proton density images (Figure 11, third and last row).

The average in-plane error for the glass needles was 0.6 mm with a maximum error of 1.4 mm, compared to 1.5 mm and 2.5 mm for the biopsy needles, which is sufficient to target the minimal clinically significant foci volume of 0.5 cc [16]. Analyzing the error reveals an average shift between glass needle void location and biopsy needle void location of 0.0 mm in the L-R direction, but 0.9 mm in the A-P direction. This shift in the A-P direction corresponds to the direction of the frequency encoding gradient of the TSE imaging sequence and is consistent with the findings reported in [42].

3) Fiber Optic Encoders Versus Mechanical Scales: The biopsy and glass needle placement accuracies reported in Section V-C1 and Section V-C2 were obtained using the fiber optic encoding system described in Section III for measuring the rotation and needle angle change of the APT II manipulator. Another twelve biopsy and glass needle placements were performed using the manual scales on the manipulator instead of the fiber optic encoders for measuring rotation and needle angle change. The average in-plane biopsy error without the encoders was 2.1 mm and the average in-plane glass needle error was 1.3 mm. The combined in-plane needle placement error using manual scales alone was 0.6 mm greater (i.e. less accurate) than when using fiber optic encoders.

D. Clinical Procedure Results

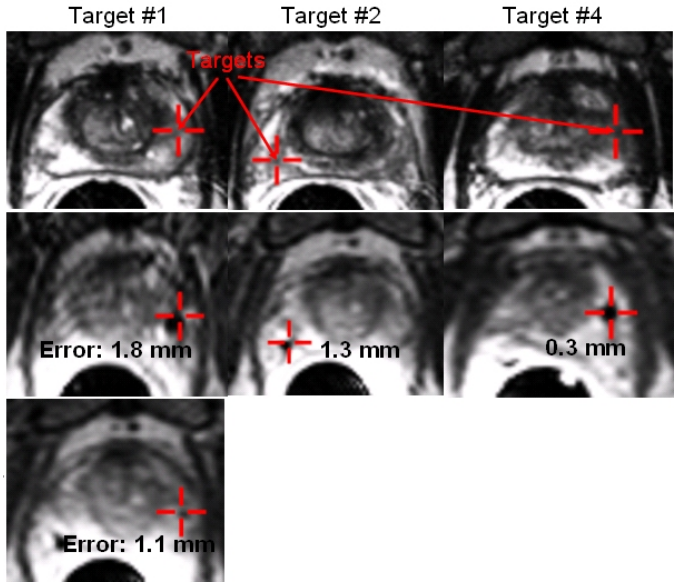

Fig. 12. Targeting images, needle visualization images, and gold marker image of the first clinical procedure using the APT II system. Confirmation images were obtained for targets 1, 2, and 4. Top image row: Suspicious targets (red cross-hairs) were selected on axial TSE T2-weighted images. Second image row: Needle tip void visualized in axial TSE proton density images. The desired targets match the actual position of the needle. Error number: The number indicates the in-plane targeting error for the needle placement. Third image row: Axial TSE proton density image showing the location of the marker placed at target location number 1.

We report the results of the first two clinical procedures performed using the APT II system. Both patients had previous positive TRUS biopsy and received treatment with external radiation beam therapy (ERBT) following the MRI-guided intervention with the APT II system. For the first patient, five biopsies of four target sites and four gold marker placements were performed. For the second patient, eight biopsies of four target sites were obtained. Both procedures were performed without use of fiber optic encoders because the fiber optic cables were too short to reach into the magnets at the time of the experiments; mechanical scales on the manipulator were used to measure the rotation and needle angle.

Figure 12 shows the accuracy results for the first patient. Four targets were selected on axial T2 weighted FSE images

(Figure 12, top row). The targets were placed at hypo-intense regions on the T2 weighted images, which represent suspicious areas for prostate cancer. One sample was procured from each of three target sites. One target was sampled twice. A gold marker was implanted at each target location after biopsy of the site. Gold markers are placed as fiducials for registration of subsequent radiation beam therapy.

Targeting accuracy of three biopsy needle placements was assessed using proton weighted axial TSE needle confirmation images (Figure 12, second row). The void created by the biopsy needle susceptibility artifact is visible close to the target. The mean in-plane targeting error for the biopsies was 1.1 mm with a maximum error of 1.8 mm. No needle confirmation image was taken from target 3, so it is omitted from Figure 12. No special marker confirmation images were obtained for this procedure. The gold marker location for target number 1 was, however, confirmed on subsequent needle confirmation images (Figure 12, third row). The distance from the center of the marker to the target location was 1.1 mm. Procedure time from start of imaging to the removal of the endorectal probe was 65 min. 14 min were used for scout and reference scans, 6 min for registration, and 15 min for acquiring reference and T2 axial images and selecting the targets. The biopsy and marker placement part of the procedure took 30 min.

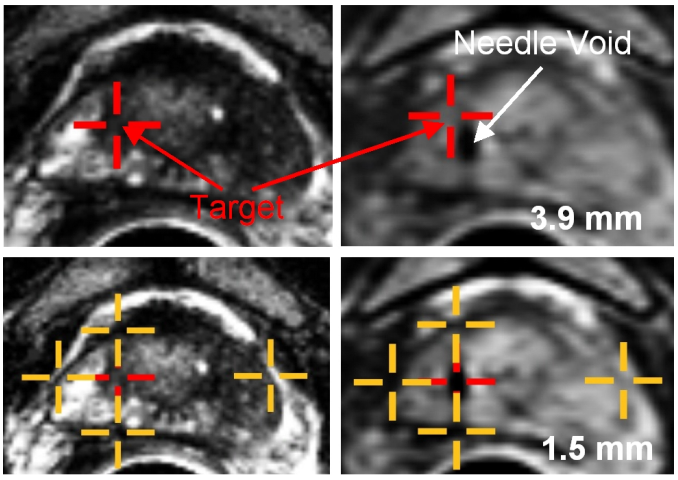

Fig. 13. Targeting image and needle confirmation image of second clinical procedure using the APT II system. Top left: Suspicious target (red cross hairs) was selected on axial TSE T2-weighted images. Top right: The needle tip void was visualized in axial TSE proton density images. Error number in top right image: The number indicates the in-plane targeting error for the needle placement of 3.9 mm. This high placement error is a result of motion of the prostate and the APT II rectal sheath, which occurred sometime in between obtaining the targeting image and confirmation image. The borders (bottom row, yellow cross hairs) of the prostate were used to calculate a 2D anatomical error. The 2D anatomical error is defined as the difference in distance of the target location to the left-right, and top-bottom prostate border on the targeting image (bottom, left) to the distance of the center of the needle void to the left-right, and top-bottom prostate border on the confirmation image (bottom, right). Error number in bottom right image: The number indicates the 2D anatomical error for the needle placement of 1.5 mm.

The pathology report revealed that the biopsy sample taken at target number 1 was positive for prostate cancer with a Gleason grade of 3+4. The patient was treated with ERBT. The implanted gold markers were used to adjust for daily set-up changes to optimize the radiation therapy [64]. In particular the area around the gold marker implanted at positive target number 1 received a higher radiation dose than the surrounding tissue, as reported in [65].

Figure 13 shows the placement accuracy results for the second patient. Needle confirmation images were obtained only for one target (Figure 13, first row). The in-plane needle placement error was calculated as 3.9 mm. Analysis of the targeting and confirmation images showed a motion shift of the prostate and the rectal sheath of the APT II occurred in between the two image sets. A 2D anatomical error was calculated using the target and needle void location in reference to the prostate border (Figure 13, bottom row). The 2D anatomical error is defined as the difference in distance of the target location to the left-right, and top-bottom prostate border on the targeting image to the distance of the center of the needle void to the left-right, and top-bottom prostate border on the confirmation image. The 2D anatomical error was calculated as 1.5 mm. The small 2D anatomical error compared to the relatively large in-plane targeting error demonstrated that similar motion occurred between the APT II manipulator and the prostate.

The out-of-plane error was not explicitly calculated for the needle placements with the APT II system. The depth of all four needle placements was well within the 15 mm long biopsy core. The pathology report revealed that the biopsy sample taken at target number 4 was positive for prostate cancer with a Gleason grade of 4+5. The procedure time for the second patient was 1h 38 min with 8 biopsies of 4 targets (two biopsies of each target). Registration took 6 min. Time from start of first biopsy to end of the procedure was 30 min.

VI. Conclusion

This paper reported the results of phantom imaging tests, detailed phantom targeting experiments, and two clinical procedures to evaluate the feasibility of performing prostate interventions with the proposed APT II system. The imaging tests show the capability of the system to obtain high resolution diagnostic images for targeted biopsy and treatment. The performance of the APT II system can be summarized as follows:

1) The APT II system demonstrated millimeter needle placement accuracy for needle biopsy and gold marker placement inside closed configuration MRI scanner in phantom targeting and initial clinical procedures.
2) The APT II system demonstrated high-resolution imaging capability with integrated endorectal imaging coil.
3) The steerable needle channel minimized prostate deformation by decoupling a stationary endorectal sheath and an internal movable needle channel under direct physician control.
4) The steerable needle channel achieved increased coverage area and eliminated obstructions of the needle channel.
5) The unrestricted 360° rotation allowed different mounting options of prone and supine patient position.
6) The hybrid tracking method eliminated the need for performing manipulator motions inside the scanner, thus

simplifying the procedure work flow and reducing procedure times.

7) The hybrid tracking method allowed for easy deployment of the APT II system on different scanners.

The observed MRI-guided needle placement accuracy is sufficient to target clinically significant prostate cancer foci (Section II-D). The errors and procedure times with the APT II system compare favorably to reported results (average in-plane biopsy error 2.7 mm and average procedure times of 76 minutes) that we achieved with the active tracking method in clinical trials using the APT-I system [1], [3]. The hybrid tracking method allows the APT II system to be used on any MRI scanner without extensive systems integration and calibration. More work in optimization of the work-flow and improvement of the imaging performance of the biopsy coil to allow reduction of scan time is needed to approach procedure times of ultrasound-guided biopsies, which are currently performed in about 20 minutes. Further clinical studies are needed to investigate the clinical performance of the reported MR guided system such as clinical accuracy and cancer yield.

ACKNOWLEDGMENTS

C. Csoma developed the targeting program with algorithms for targeting and fiducial marker tracking developed by A. Krieger. G. Metzger helped with evaluation of the hybrid tracking method. D. Qian built the first two endorectal imaging coils for the APT II system. N. Shanmugaratnam, G. Thevathasan, C. Piron, and H. Wang from Sentinelle Medical provided help with developing, building, and testing of the endorectal imaging coils designed to limit RF heating. The manipulator of the APT II system was fabricated by M. Franckowiak and W. Krug. A. Blank helped with the fiber optic encoders.

REFERENCES

[1] A. Krieger, R. C. Susil, C. Ménard, J. A. Coleman, G. Fichtinger, E. Atalar, and L. L. Whitcomb, "Design of a novel MRI compatible manipulator for image guided prostate interventions," *IEEE Transactions on Biomedical Engineering*, vol. 52, no. 2, pp. 306–313, Feb. 2005.

[2] C. Ménard, R. C. Susil, P. Choyke, J. Coleman, R. Grubb, A. Gharib, A. Krieger, P. Guion, D. Thomasson, K. Ullman, S. Gupta, V. Espina, L. Liotta, E. Petricoin, G. Fitchtinger, L. L. Whitcomb, E. Atalar, C. Norman Coleman, and K. Camphausen, "An interventional magnetic resonance imaging technique for the molecular characterization of intraprostatic dynamic contrast enhancement," *Molecular Imaging*, vol. 4, no. 1, pp. 63–66, 2005.

[3] R. C. Susil, C. Ménard, A. Krieger, J. A. Coleman, K. Camphausen, P. Choyke, G. Fichtinger, L. L. Whitcomb, C. N. Coleman, and E. Atalar, "Transrectal prostate biopsy and fiducial marker placement in a standard 1.5 T magnetic resonance imaging scanner." *Journal of Urology*, vol. 175, no. 1, pp. 113–120, Jan 2006.

[4] A. Krieger, G. Metzger, G. Fichtinger, E. Atalar, and L. L. Whitcomb, "A hybrid method for 6-DOF tracking of MRI-compatible robotic interventional devices," in *Proceedings - IEEE International Conference on Robotics and Automation*, vol. 2006, Orlando, FL, United States, May 2006, pp. 3844–3849.

[5] American Cancer Society, *Cancer Facts and Figures 2010*. Atlanta: American Cancer Society, 2010.

[6] S. Haker, R. Mulkern, J. Roebuck, A. Barnes, S. DiMaio, N. Hata, and C. Tempany, "Magnetic resonance-guided prostate interventions," *Topics in Magnetic Resonance Imaging*, vol. 16, no. 5, p. 355, 2005.

[7] P. Gann, A. Fought, R. Deaton, W. Catalona, and E. Vonesh, "Risk factors for prostate cancer detection after a negative biopsy: A novel multivariable longitudinal approach," *Journal of Clinical Oncology*, vol. 28, no. 10, p. 1714, 2010.

[8] J. C. Presti, "Prostate cancer: assessment of risk using digital rectal examination, tumor grade, prostate-specific antigen, and systematic biopsy." *Radiologic Clinics of North America*, vol. 38, no. 1, pp. 49–58, Jan 2000.

[9] M. K. Terris, E. M. Wallen, and T. A. Stamey, "Comparison of midlobe versus lateral systematic sextant biopsies in the detection of prostate cancer." *Urologia Internationalis*, vol. 59, no. 4, pp. 239–242, 1997.

[10] K. A. Roehl, J. A. V. Antenor, and W. J. Catalona, "Serial biopsy results in prostate cancer screening study." *Journal of Urology*, vol. 167, no. 6, pp. 2435–2439, Jun 2002.

[11] M. Norberg, L. Egevad, L. Holmberg, P. Sparén, B. J. Norlén, and C. Busch, "The sextant protocol for ultrasound-guided core biopsies of the prostate underestimates the presence of cancer." *Urology*, vol. 50, no. 4, pp. 562–566, Oct 1997.

[12] F. Rabbani, N. Stroumbakis, B. R. Kava, M. S. Cookson, and W. R. Fair, "Incidence and clinical significance of false-negative sextant prostate biopsies." *Journal of Urology*, vol. 159, no. 4, pp. 1247–1250, Apr 1998.

[13] A. E. Wefer, H. Hricak, D. B. Vigneron, F. V. Coakley, Y. Lu, J. Wefer, U. Mueller-Lisse, P. R. Carroll, and J. Kurhanewicz, "Sextant localization of prostate cancer: comparison of sextant biopsy, magnetic resonance imaging and magnetic resonance spectroscopic imaging with step section histology." *Journal of Urology*, vol. 164, no. 2, pp. 400–404, Aug 2000.

[14] A. V. Taira, G. S. Merrick, R. W. Galbreath, H. Andreini, W. Taubenslag, R. Curtis, W. M. Butler, E. Adamovich, and K. E. Wallner, "Performance of transperineal template-guided mapping biopsy in detecting prostate cancer in the initial and repeat biopsy setting." *Prostate Cancer Prostatic Dis*, vol. 13, no. 1, pp. 71–77, Mar 2010.

[15] M. K. Terris, "Strategies for repeat prostate biopsies." *Curr Urol Rep*, vol. 10, no. 3, pp. 172–178, May 2009.

[16] J. B. Bak, S. K. Landas, and G. P. Haas, "Characterization of prostate cancer missed by sextant biopsy." *Clinical Prostate Cancer*, vol. 2, no. 2, pp. 115–118, Sep 2003.

[17] T. Goossen and H. Wijkstra, "Transrectal ultrasound imaging and prostate cancer." *Arch Ital Urol Androl*, vol. 75, no. 1, pp. 68–74, Mar 2003.

[18] B. Djavan and M. Margreiter, "Biopsy standards for detection of prostate cancer." *World J Urol*, vol. 25, no. 1, pp. 11–17, Mar 2007.

[19] H. Welch, E. Fisher, D. Gottlieb, and M. Barry, "Detection of Prostate Cancer via Biopsy in the Medicare–SEER Population During the PSA Era," *Journal of the National Cancer Institute*, vol. 99, no. 18, p. 1395, 2007.

[20] K. K. Yu and H. Hricak, "Imaging prostate cancer." *Radiologic Clinics of North America*, vol. 38, no. 1, pp. 59–85, viii, Jan 2000.

[21] K. M. Pondman, J. J. Ftterer, B. ten Haken, L. J. S. Kool, J. A. Witjes, T. Hambrock, K. J. Macura, and J. O. Barentsz, "MR-guided biopsy of the prostate: an overview of techniques and a systematic review." *Eur Urol*, vol. 54, no. 3, pp. 517–527, Sep 2008.

[22] J. J. Ftterer, J. Barentsz, and S. T. Heijmijnk, "Imaging modalities for prostate cancer." *Expert Rev Anticancer Ther*, vol. 9, no. 7, pp. 923–937, Jul 2009.

[23] H. Elhawary, Z. T. H. Tse, A. Hamed, M. Rea, B. L. Davies, and M. U. Lamperth, "The case for MR-compatible robotics: a review of the state of the art." *International Journal of Medical Robotics and Computer Assisted Surgery*, vol. 4, no. 2, pp. 105–113, Jun 2008.

[24] S. Adusumilli and E. S. Pretorius, "Magnetic resonance imaging of prostate cancer." *Seminars in Urologic Oncology*, vol. 20, no. 3, pp. 192–210, Aug 2002.

[25] H. H. Quick, J. M. Serfaty, H. K. Pannu, R. Genadry, C. J. Yeung, and E. Atalar, "Endourethral MRI." *Magnetic Resonance in Medicine*, vol. 45, no. 1, pp. 138–146, Jan 2001.

[26] C. Ménard, I. C. Smith, R. L. Somorjai, L. Leboldus, R. Patel, C. Littman, S. J. Robertson, and T. Bezabeh, "Magnetic resonance spectroscopy of the malignant prostate gland after radiotherapy: a histopathologic study of diagnostic validity." *International J. of Radiation Oncology Biology Physics*, vol. 50, no. 2, pp. 317–323, Jun 2001.

[27] I. Chan, W. Wells, R. V. Mulkern, S. Haker, J. Zhang, K. H. Zou, S. E. Maier, and C. M. C. Tempany, "Detection of prostate cancer by integration of line-scan diffusion, T2-mapping and T2-weighted magnetic resonance imaging; a multichannel statistical classifier." *Medical Physics*, vol. 30, no. 9, pp. 2390–2398, Sep 2003.

[28] C.-F. Westin, S. E. Maier, H. Mamata, A. Nabavi, F. A. Jolesz, and R. Kikinis, "Processing and visualization for diffusion tensor MRI." *Medical Image Analysis*, vol. 6, no. 2, pp. 93–108, Jun 2002.

[29] R. C. Susil, A. Krieger, J. A. Derbyshire, A. Tanacs, L. L. Whitcomb, G. Fichtinger, and E. Atalar, "System for MR image-guided prostate

interventions: Canine study," *Radiology*, vol. 228, no. 3, pp. 886–894, September 2003.

[30] S. L. Chowning, R. C. Susil, A. Krieger, G. Fichtinger, L. L. Whitcomb, and E. Atalar, "A preliminary analysis and model of prostate injection distributions." *Prostate*, vol. 66, no. 4, pp. 344–357, Mar 2006.

[31] A. V. D'Amico, C. M. Tempany, R. Cormack, N. Hata, M. Jinzaki, K. Tuncali, M. Weinstein, and J. P. Richie, "Transperineal magnetic resonance image guided prostate biopsy." *Journal of Urology*, vol. 164, no. 2, pp. 385–387, Aug 2000.

[32] J. C. Chen, J. A. Moriarty, J. A. Derbyshire, R. D. Peters, J. Trachtenberg, S. D. Bell, J. Doyle, R. Arrelano, G. A. Wright, R. M. Henkelman, R. S. Hinks, S. Y. Lok, A. Toi, and W. Kucharczyk, "Prostate cancer: MR imaging and thermometry during microwave thermal ablation-initial experience." *Radiology*, vol. 214, no. 1, pp. 290–297, Jan 2000.

[33] S. J. Graham, G. J. Stanisz, A. Kecojevic, M. J. Bronskill, and R. M. Henkelman, "Analysis of changes in MR properties of tissues after heat treatment." *Magnetic Resonance in Medicine*, vol. 42, no. 6, pp. 1061–1071, Dec 1999.

[34] R. Susil, A. Krieger, J. Derbyshire, A. Tanacs, L. Whitcomb, G. Fichtinger, and E. Atalar, "A system for guidance and monitoring of transrectal prostate biopsy in a 1.5 T closed MR scanner," *European Radiology*, vol. 12(9), 2002.

[35] A. Krieger, R. Susil, A. Tanacs, G. Fichtinger, L. Whitcomb, and E. Atalar, "A MRI compatible device for MRI guided transrectal prostate biopsy," *International Society of MRI in Medicine, 10th Scientific Meeting, Honolulu*, p. 338, 2002.

[36] D. Beyersdorff, A. Winkel, B. Hamm, S. Lenk, S. A. Loening, , and M. Taupitz, "MR imaging-guided prostate biopsy with a closed MR unit at 1.5 T: Initial results," *Radiology*, vol. 234, no. 2, pp. 576–581, February 2005.

[37] K. Engelhard, H. P. Hollenbach, B. Kiefer, A. Winkel, K. Goeb, and D. Engehausen, "Prostate biopsy in the supine position in a standard 1.5-T scanner under real time MR-imaging control using a MR-compatible endorectal biopsy device." *European Radiology*, vol. 16, no. 6, pp. 1237–1243, Jun 2006.

[38] J. Futterer, M. Schouten, T. Scheenen, and J. Barentsz, "MR-compatible transrectal prostate biopsy robot: A feasibility study," in *16th Annual ISMRM Scientific Meeting and Exhibition*. ISMRM, 2010.

[39] H. Elhawary, A. Zivanovic, M. Rea, B. Davies, C. Besant, D. McRobbie, N. de Souza, I. Young, and M. Lamperth, "The feasibility of MR-image guided prostate biopsy using piezoceramic motors inside or near to the magnet isocentre." *International Conference on Medical Image Computing and Computer-Assisted Intervention*, vol. 9, no. Pt 1, pp. 519–526, 2006.

[40] R. C. Susil, K. Camphausen, P. Choyke, E. R. McVeigh, G. S. Gustafson, H. Ning, R. W. Miller, E. Atalar, C. N. Coleman, and C. Ménard., "System for prostate brachytherapy and biopsy in a standard 1.5 T MRI scanner," *Magnetic Resonance in Medicine*, vol. 52, no. 3, pp. 683–7, September 2004.

[41] K. Chinzei, N. Hata, F. A. Jolesz, and R. Kikinis, "MRI compatible surgical assist robot: System integration and preliminary feasibility study," in *Medical Image Computing and Computer-Assisted Intervention (MICCAI)*, vol. 1935, October 2000, pp. 921–930.

[42] S. P. DiMaio, S. Pieper, K. Chinzei, N. Hata, S. J. Haker, D. F. Kacher, G. Fichtinger, C. M. Tempany, and R. Kikinis, "Robot-assisted needle placement in open MRI: system architecture, integration and validation." *Comput Aided Surgery*, vol. 12, no. 1, pp. 15–24, Jan 2007.

[43] K. Tadakuma, L. DeVita, S. Y., and S. Dubowsky, "The experimental study of a precision parallel manipulator with binary actuation: With application to MRI cancer treatment," in *Proc. IEEE International Conference on Robotics and Automation ICRA '08*, May 21–May 23, 2008, pp. 2503–2508.

[44] J. Plante, L. Devita, K. Tadakuma, and S. Dubowsky, *MRI Compatible Device for Robotic Assisted Interventions to Prostate Cancer, in Biomedical Applications of Electroactive Polymer Actuators*. John Wiley and Sons, 2009, ch. 22, doi:10.1002/9780470744697.ch22.

[45] D. Stoianovici, D. Song, D. Petrisor, D. Ursu, D. Mazilu, M. Muntener, M. Mutener, M. Schar, and A. Patriciu, "MRI stealth robot for prostate interventions." *Minimally Invasive Therapy and Allied Technologies*, vol. 16, no. 4, pp. 241–248, 2007.

[46] G. S. Fischer, I. Iordachita, C. Csoma, J. Tokuda, S. P. DiMaio, C. M. Tempany, N. Hata, and G. Fichtinger, "MRI-compatible pneumatic robot for transperineal prostate needle placement," *IEEE/ASME Transactions on Mechatronics*, vol. 13, no. 3, pp. 295–305, Jun. 2008.

[47] S.-E. Song, N. B. Cho, G. Fischer, N. Hata, C. Tempany, G. Fichtinger, and I. Iordachita, "Development of a pneumatic robot for MRI-guided transperineal prostate biopsy and brachytherapy: New approaches," in *Proc. IEEE Int Robotics and Automation (ICRA) Conf*, 2010, pp. 2580–2585.

[48] A. A. Goldenberg, J. Trachtenberg, W. Kucharczyk, Y. Yi, M. Haider, L. Ma, R. Weersink, and C. Raoufi, "Robotic system for closed-bore MRI-guided prostatic interventions," *IEEE/ASME Transactions on Mechatronics*, vol. 13, no. 3, pp. 374–379, Jun. 2008.

[49] M. R. van den Bosch, M. R. Moman, M. van Vulpen, J. J. Battermann, E. Duiveman, L. J. van Schelven, H. de Leeuw, J. J. W. Lagendijk, and M. A. Moerland, "MRI-guided robotic system for transperineal prostate interventions: proof of principle." *Phys Med Biol*, vol. 55, no. 5, pp. N133–N140, Mar 2010.

[50] S. Zangos, K. Eichler, K. Engelmann, M. Ahmed, S. Dettmer, C. Herzog, W. Pegios, A. Wetter, T. Lehnert, M. G. Mack, and T. J. Vogl, "MR-guided transgluteal biopsies with an open low-field system in patients with clinically suspected prostate cancer: technique and preliminary results." *European Radiology*, vol. 15, no. 1, pp. 174–182, Jan 2005.

[51] S. Zangos, C. Herzog, K. Eichler, R. Hammerstingl, A. Lukoschek, S. Guthmann, B. Gutmann, U. J. Schoepf, P. Costello, and T. J. Vogl, "MR-compatible assistance system for punction in a high-field system: device and feasibility of transgluteal biopsies of the prostate gland." *European Radiology*, vol. 17, no. 4, pp. 1118–1124, Apr 2007.

[52] T. Vogl, H. Mayer, S. Zangos, J. Selby, H. Ackermann, and F. Mayer, "Prostate Cancer: MR Imaging-guided Galvanotherapy–Technical Development and First Clinical Results1," *Radiology*, vol. 245, no. 3, p. 895, 2007.

[53] D. F. Gleason, "Classification of prostatic carcinomas." *Cancer Chemotherapy Reports. Part 1.*, vol. 50, no. 3, p. 125, 1966.

[54] J. E. McNeal, D. G. Bostwick, R. A. Kindrachuk, E. A. Redwine, F. S. Freiha, and T. A. Stamey, "Patterns of progression in prostate cancer." *Lancet*, vol. 1, no. 8472, pp. 60–63, Jan 1986.

[55] T. A. Stamey, F. S. Freiha, J. E. McNeal, E. A. Redwine, A. S. Whittemore, and H. P. Schmid, "Localized prostate cancer. relationship of tumor volume to clinical significance for treatment of prostate cancer." *Cancer*, vol. 71, no. 3 Suppl, pp. 933–938, Feb 1993.

[56] W. A. Kaiser, H. Fischer, J. Vagner, and M. Selig, "Robotic system for biopsy and therapy of breast lesions in a high-field whole-body magnetic resonance tomography unit." *Investigative Radiology*, vol. 35, no. 8, pp. 513–519, Aug 2000.

[57] A. Felden, J. Vagner, A. Hinz, H. Fischer, S. Pfleiderer, J. Reichenbach, and W. Kaiser., "ROBITOM-robot for biopsy and therapy of the mamma." *Biomedizinische Technik - Biomedical Engineering (Berlin).*, vol. 47, no. Suppl 1, pp. Pt 1:2–5, 2002.

[58] S. Hushek, B. Fetics, and R. Moser, "Initial clinical experience with a passive electromagnetic 3D locator system," in *5th Interventional MRI Symposium, Boston, October15-16, Proceedings*, 2004.

[59] C. L. Dumoulin, S. P. Souza, and R. D. Darrow, "Real-time position monitoring of invasive devices using magnetic resonance," *Magnetic Resonance in Medicine*, vol. 29, no. 3, pp. 411–415, March 1993.

[60] G. Golub and C. Van Loan, *Matrix computations*. Johns Hopkins University Press, 1996, third Edition.

[61] T. De Silva, A. Fenster, J. Samarabandu, and A. Ward, "Quantification of Prostate Deformation due to Needle Insertion during TRUS-guided Biopsy," *Medical Image Computing and Computer-Assisted Intervention–MICCAI 2010*, pp. 213–220, 2010.

[62] H. Xu, A. Lasso, S. Vikal, P. Guion, A. Krieger, A. Kaushal, L. L. Whitcomb, and G. Fichtinger, "Accuracy validation for MRI-guided robotic prostate biopsy," in *Medical Imaging 2010: Visualization, Image-Guided Procedures, and Modeling*, SPIE. San Diego, California, USA: SPIE, 2010, pp. 762 517 – 762 517–8.

[63] NEMA, *Determination of Signal-to-Noise Ratio (SNR) in Diagnostic Magnetic Resonance Imaging, NEMA Standard Publication MS 1-2008*. The Association of Electrical and Medical Imaging Equipment Manufacturers, 2008.

[64] G. Pang, D. Beachey, P. O'Brien, and J. Rowlands, "Imaging of 1.0-mm-diameter radiopaque markers with megavoltage X-rays: an improved online imaging system," *International Journal of Radiation Oncology Biology Physiscs*, vol. 52, no. 2, pp. 532–537, February 2002.

[65] A. K. Singh, P. Guion, N. Sears-Crouse, K. Ullman, S. Smith, P. S. Albert, G. Fichtinger, P. L. Choyke, S. Xu, J. Kruecker, B. J. Wood, A. Krieger, and H. Ning, "Simultaneous integrated boost of biopsy proven, MRI defined dominant intra-prostatic lesions to 95 Gray with IMRT: early results of a phase I NCI study." *Radiation Oncology*, vol. 2, p. 36, 2007.

Axel Krieger (M'05) received his Ph.D. in mechanical engineering from the Johns Hopkins University in 2008. Currently he is Product Leader, Prostate Solutions at Sentinelle Medical in Toronto, Canada, a Hologic Division. His research interest focuses on the development of MRI compatible coils and devices for MRI-guided interventions. He has been a member of IEEE since 2005.

Iulian I. Iordachita (M'08) received the B.Eng. degree in mechanical engineering, the M.Eng. degree in industrial robots, and the Ph.D. degree in mechanical engineering in 1984, 1989, and 1996, respectively, from the University of Craiova, Craiova, Romania. He is an Assistant Research Professor at the Department of Mechanical Engineering and the Laboratory for Computational Sensing and Robotics, Johns Hopkins University, Baltimore, MD, where he is engaged in research on robotics, in particular, robotic hardware. His current research interests include design and manufacturing of surgical instrumentation and devices, medical robots, and mechanisms and mechanical transmissions for robots.

Peter Guion Peter Guion (M'05) received his MS degree in Aerospace Engineering from the University of Maryland, College Park in 2003. He has also earned BS degrees in Mechanical and Electrical Engineering from Virginia Tech (1996) and the University of Maryland, College Park (1999), respectively. He is the staff engineer at the Radiation Oncology Branch, National Cancer Institute in Bethesda, MD. His research is in robotics and control systems, with a focus on MRI-guided procedures.

Anurag K. Singh M.D. received his M.D. degree from Washington University, Saint Louis in 1999. He is an Associate Professor, Residency Program Director, and Director of Research in the department of Radiation Medicine at Roswell Park Cancer Institute, Buffalo, NY, USA. His research interests include imaging and organ motion research to better define tumor extent and minimize normal tissue irradiation and biological modifiers (to enhance efficacy or limit toxicity of radiation.)

Aradhana Kaushal M.D. graduated with a B.A./M.D. degree, magna cum laude, from Boston University. She completed a year at the National Cancer Institute conducting research under the direction of Drs. Norman Coleman and David Gius, studying mechanisms for resistance of tumor cells to oxidative stress. She completed her internship in internal medicine at Lenox Hill Hospital, a teaching hospital of New York University and a residency in radiation oncology at Thomas Jefferson University Hospital, also serving as chief resident during her last year of residency. Her current clinical focus is prostate and pediatric malignancies. Dr. Kaushal is board certified by the ABR. Dr. Kaushal is board certified by the American Board of Radiology.

Cynthia Ménard M.D. received her M.D. from the University of Calgary in 1996, and completed her residency in Radiation Oncology at the University of Alberta, Edmonton, in 2001. She then pursued post-graduate research training as a Fellow in the Radiation Oncology Branch of the National Cancer Institute (NIH) until 2003. She is currently appointed as a Clinician Scientist in the Radiation Medicine Program at Princess Margaret Hospital, and Associate Professor in the Department of Radiation Oncology, University of Toronto. The primary focus of her scholarly activity is to better individualize radiation therapy through the development, validation, and clinical application of MRI techniques to radiation treatment planning, response assessment, and treatment adaptation.

Peter A Pinto M.D. is a Senior Investigator and faculty member in the Urologic Oncology Branch of the National Cancer Institute, National Institutes of Health, Bethesda, MD. Following a residency in Urologic Surgery at Long Island Jewish Medical Center–Albert Einstein College of Medicine in New York, he was a Fellow and Clinical Instructor at the Brady Urologic Institute, Johns Hopkins Hospital. Dr. Pinto is a Board Certified Urologic Surgeon specializing in oncology and is Director of the Urologic Oncology Fellowship Program at the National Cancer Institute. He is nationally and internationally recognized as an expert in minimally invasive treatment of urologic cancers, specializing in laparoscopic and robotic surgery for prostate, kidney, bladder, and testicular cancer.

Kevin Camphausen M.D. received his undergraduate degree from Purdue University in 1988. He then completed his MD (1996) and medical internship (1997) at Georgetown University Medical Center. He next completed his residency in radiation oncology at the Joint Center of Radiation Therapy at Harvard Medical School (2001). While there, he worked in the laboratory of Dr. Judah Folkman studying the interactions of antiangiogenic therapy and radiotherapy. He joined the Radiation Oncology Branch in 2001 as a tenure track investigator. He has recently received tenure at the NIH (2007) and was promoted to be the Chief of the Radiation Oncology Branch (ROB), Center for Cancer Research (CCR), NCI (2007). He is a physician/scientist who has a laboratory program focusing on the development and characterization of agents that alter the tumoral response to radiation. He has been successful in translating his work from the laboratory to the clinic. Dr. Camphausen is an internationally recognized leader in his field and an expert in the field of drug-induced tumor radiosensitization including the use of anti-angiogenic agents in combination with radiotherapy.

Gabor Fichtinger (M'04) received a Ph.D. degree in computer science from the Technical University of Budapest, Hungary in 1990. He is Professor in the School of Computing, with cross appointments in the Departments of Mechanical and Material Engineering, Electrical and Computer Engineering, and Surgery, at Queen's University, Kingston, Canada, where he directs the Percutaneous Surgery Laboratory. His research specializes on system development for computer-assisted interventions, with special focus on image-guided oncology applications. He holds a Level-1 Cancer Care Ontario Research Chair in Cancer Imaging.

Louis L. Whitcomb (S'86-M'95-SM'02-F'11) received a Ph.D. degree in electrical engineering from Yale University 1992. He is Professor in the Department of Mechanical Engineering, with secondary appointment in the Department of Computer Science, Johns Hopkins University, Baltimore, MD, USA, where he directs JHU's Laboratory for Computational Sensing and Robotics. His research is on the design, dynamics, and control of robotic systems, with focus on image guided systems for intervention in extreme environments, with focus on MRI-guided international systems. He is the Louis R. Sardella Faculty Scholar and a Fellow of the IEEE.